Geomechanics and Engineering, *Vol. 42, No. 2 (2025) 93-105*
https://doi.org/10.12989/gae.2025.42.2.093

Study on the influence of groundwater table rebound on tunnel structure: A case study from Xiangshan tunnel

Xiaoxu Tian[1,2a], Zhanping Song*[1,2], Hongwei Pan[3b] and Jun Li[3c]

[1]*School of Civil Engineering, Xi'an University of Architecture and Technology, Xi'an 710055, China*
[2]*Shaanxi Key Laboratory of Geotechnical and Underground Space Engineering, Xi'an 710055, China*
[3]*The First Engineering Co., Ltd of China Railway Beijing Engineering Bureau Group, Xi'an 710199, China*

(*Received December 11, 2024, Revised June 25, 2025, Accepted July 2, 2025*)

Abstract. The surface pre-dewatering is usually carried out before the excavation of the tunnel within water-rich fine sand stratum. Due to the high cost of surface pre-dewatering, the area of the tunnel that has been applied for the first lining may not continue to pre-dewatering, and the groundwater level will rise again. Under the influence of rising groundwater level, the first lining of the tunnel may appear large deformation and cracking phenomenon. Taking Xiangshan Tunnel as an engineering case, the influence of groundwater level rise on tunnel supporting structure was was investigated. Firstly, the main engineering problems faced in the construction and the corresponding dewatering measures were reviewed. Then the deformation of surrounding rock, contact pressure, stress and groundwater level in the construction process were monitored and analyzed. The groundwater level rebound will cause large vertical settlement of the first lining and large extrusion deformation of the tunnel face. When the groundwater level reaches the arch waist, the minimum principal stress at the first lining arch foot exceeds its ultimate strength, and it will crack and fail. The increase of surrounding rock moisture content caused by groundwater rebound is the main reason leading to the failure of the first lining. Reducing the groundwater level, adding steel arch to the damaged section of the first lining and carrying out radial grouting can effectively solve the problem of first lining cracking. The experience and lessons learned in the construction process of Xiangshan can provide reference for similar projects in recent years.

Keywords: groundwater table rebound; deformation characteristics; surrounding rock pressure; tunnels; water-rich fine sand stratum

1. Introduction

In recent years, water-rich fine sand strata have frequently been encountered in tunnel construction in coastal cities, Gansu, Ningxia and other regions of China (Tian *et al.* 2022). Water-rich fine sand is generally light red, with fine-grained structure. Its overall stability is better under dry conditions (Wang *et al.* 2024). When exposed to water infiltration or immersion, it often appears as a flow deformation under the disturbance of construction, and the engineering properties are poor (Khezri *et al.* 2010, Chen *et al.* 2018). In order to improve the stability of surrounding rocks, pre-dewatering was usually carried out before tunnel excavation (Ding *et al.* 2012). Due to the high cost of pre-dewatering, the groundwater table will rise again in the area where the tunnel has been supported by the first lining. Under the influence of groundwater table rising, deformation and cracking often may appear large deformation and cracking phenomenon, which seriously threatens the safety of tunnel construction(Zhang *et al.* 2021, Tian *et al.* 2021, Qiu *et al.* 2024). Therefore, it is of great practical significance to study the effect of groundwater rebound on tunnel first lining.

At present, the research on tunnels within water-rich fine sand mainly focuses on the analysis of disaster mechanism (Kirsch 2010, Zan *et al.* 2024, Yang *et al.* 2018, Cheng *et al.* 2023, Yang *et al.* 2022). According to the analysis of laboratory test and field test, Liang *et al.* (2020) found that the properties of fine sand, slurry circulation quality, support pressure setting and excess pore water pressure fluctuation are the main causes of ground collapse caused by shield construction in water-rich fine silty sand. Liu *et al.* (2018) conducted research on deformation characteristics and collapse mechanisms of water- rich soil tunnels, and found that geological conditions and construction factors were the main causes of deformation and collapse of the tunnels. Yin *et al.* (2020) analyzed the distribution of soil movement, ground movement, tunnel face support force and micro-contact in the process of progressive failure of the sand tunnel face, and found that particle shape has a significant effect on progressive failure.

However, some scholars believe that the stability of the tunnel face is the key factor to control the stability of the tunnel. Therefore, they have analyzed the stability of the tunnel face, and proposed the failure mode of the tunnel face and the calculation model of the limit support pressure respectively (Eskandari *et al.* 2018, Park 2019, Li *et al.*

*Corresponding author, Professor
E-mail: songzhpyt@xauat.edu.cn
[a]Lecturer
[b]Senior engineer
[c]Senior engineer

Copyright © 2025 Techno-Press, Ltd.

ISSN: 2005-307X (Print), 2092-6219 (Online)

2023). For example, Long and Tan (2020) studied the geological disasters and failure mechanisms of tunnel leakage in water-rich fine silty sand strata through experiments and numerical simulations. It is found that the stress changes around the tunnel caused by permeation erosion are similar to the results of active gate tests, and a stress arch model considering tunnel seepage erosion is proposed. Wang *et al.* (2019) studied the axisymmetric problem of the stability of the water-rich sandy shield tunnel face under seepage conditions, and proposed a theoretical analysis model to determine the failure mode of the tunnel face and the limit support pressure.

Some other scholars also believed that the deformation control technology of water-rich fine sand tunnel is the key to the problem (Lei *et al.* 2020, Fan *et al.* 2023). Therefore, they proposed and introduced the deformation control technology of the grouting reinforcement and freezing reinforcement. Liu *et al.* (2019) theoretically analyzed and numerically calculated the grouting process of the sleeve valve pipe in the fine sand stratum, and determined the relationship between the grouting pressure, the diffusion radius and the initial fracture pressure. Ye *et al*. (2019) took the first subway shield tunnel under the Yellow River in China (East Lanzhou Yellow River Tunnel) as an engineering case, summarized the key technology of the cutterhead design and modification scheme suitable for the sand-cobble stratum and the slurry film formation for crossing the sand pit. Kang *et al.* (2016) studied the construction method and the stability of the tunnel face of the Gongbei Tunnel. The evolution law of temperature field, freezing construction scheme, freezing wall thickening and optimal freezing time were determined when the thickness of the frozen wall was determined. A three-dimensional model of freezing sealing and combined construction method for tunnels in soft soil foundation of coastal cities was proposed. Oreste and Dias (2012) introduced a calculation method for the reinforcement of glass fiber reinforced plastic piles at the tunnel face, which is used to stabilize the tunnel face. Song *et al*. (2020) provided a construction method suitable for water-rich fine sand tunnel.

In summary, the current research on tunnels with water-rich fine sand mainly focuses on the disaster mechanism and stability analysis of tunnel face, as well as the grouting reinforcement and deformation control mechanism. There are few studies on the influence of groundwater rebound on tunnel structures. Therefore, this study took the Xiangshan Tunnel as an engineering case, first reviews the main engineering problems faced during the construction, as well as the corresponding dewatering measures. Then, the deformation of the surrounding rock, the contact pressure and stress of the liner, and the change law of the groundwater table during the construction process were monitored and analyzed. Finally, based on numerical experiments, the distribution characteristics of the first lining deformation under the influence of groundwater rebound were analyzed, and the reasons for the failure of the tunnel's first lining caused by groundwater table rebound were clarified.

2. Project background

2.1 Project overview

The Xiangshan Tunnel is located in Zhongwei City, Ningxia, with a total length of 17763.3 m. It is a double-track tunnel with a spacing of 4.6 m. The tunnel is 14.38 m wide and 12.24 m high, with a maximum buried depth of about 380 m. The tunnel site is in a low-medium mountain area with strong terrain cutting and valley development. The surrounding rock of the DK43+958~DK44+515 section of Xiangshan Tunnel is fully weathered sandstone mixed with mudstone, with poor diagenesis. The DK43+925 ~ DK44+515 section of Xiangshan Tunnel is constructed by the three-step reserved core soil method. The excavation height of the upper step is 4.2 m, the length of the upper step is 5 m, the height of the middle step is 3.5 m, and the length of the middle step is 10 m. The lower step and inverted arch are closed in time to form a loop. The distance from the tunnel face to the closed loop of the first lining is less than 35 m. The first lining adopts 25a I-steel, with a thickness of sprayed concrete of 28 cm and a spacing of steel frames of 60 cm.

2.2 Dewatering measures

The Xiangshan Tunnel DK43+925~DK44+515 section belongs to the water-rich area. The buried depth of groundwater is about 60.2 m~73.6 m, and the tunnel is located about 49 m below the groundwater table. The surrounding rock has high water content, poor self-stability, high fluidity, large tunnel settlement deformation and easy collapse, so the construction difficulty is great. Therefore, before tunnel construction, it is necessary to reduce the groundwater table. The dewatering well is symmetrically on the left and right sides of the tunnel. The distance between the dewatering well and the outer contour of the first lining of the tunnel is 5 m, and the unilateral spacing of the dewatering well along the line direction is 16 m, and the spacing between the two sides is 8 m. It is alternately arranged along the left and right sides of the tunnel. The schematic diagram of the layout of the well location is shown in Figs. 1(a) and 1(c). The dewatering well includes water extraction pipe, sand settlement pipe, pump, filter pipe, small gravel, etc. The drilling diameter is 600 mm, the well pipe diameter is 300 mm, and the well depth is 20 m below the inverted arch.

It was found during the actual construction process that the phenomenon of cracking and even falling of the first lining frequently occurred in the area where the first lining had been constructed, as shown in Fig. 1(d). Through on-site water level monitoring and actual investigation, it was found that as the tunnel construction gradually moved forward, the groundwater table in the completed first lining section no longer decreased. The groundwater table in the area where the first lining had been constructed would gradually rise, and the increase in water content in the surrounding rock in the first lining area may lead to the deterioration of the mechanical parameters of the surrounding rock, which may be the cause of large

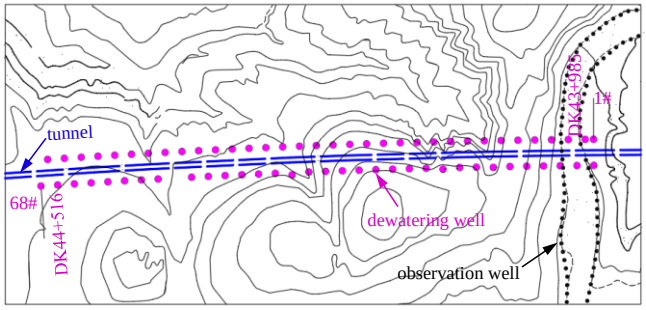

(a) Tunnel plane and dewatering well layout

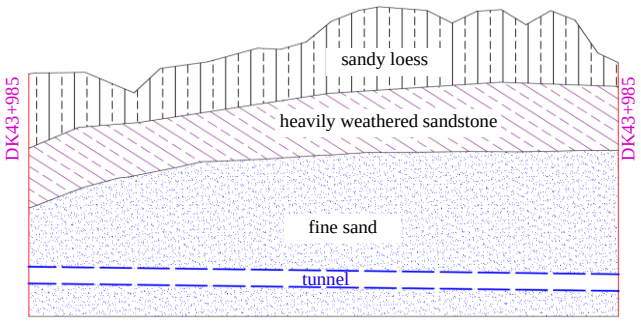

(b) Tunnel geological profile

Dewatering well

Water-collecting well

(c) Dewatering measures

Sand boil

First lining failure

(d) Disaster type

Fig. 1 Tunnel plane, geological profile and engineering problems

Fig. 2 Layout of monitoring points

deformation, cracking, falling, and even failure of the first lining. Therefore, the influence of groundwater table rise on tunnel first lining was analyzed through on-site monitoring data and numerical simulation results.

3. Monitoring data

3.1 Layout of monitoring points

To explore the evolution law of tunnel deformation and stress during tunnel construction, an first lining deformation evolution analysis was conducted by selecting a monitoring section every 10 m along the tunnel longitudinal direction within the range of DK44+020~050. Within the range of DK44+000~100, a section was selected every 10 m to analyze the final settlement and convergence. 8 monitoring points were set at the arch foot, side wall, arch shoulder and vault of the liner to monitor the pressure and internal stress of the liner. The DK43+981.3 section and DK44+009.3 section were selected for stress monitoring of the liner, and the layout of the monitoring points is shown in Fig. 2.

3.2 Surrounding rock deformation

3.2.1 Vault settlement and horizontal convergence

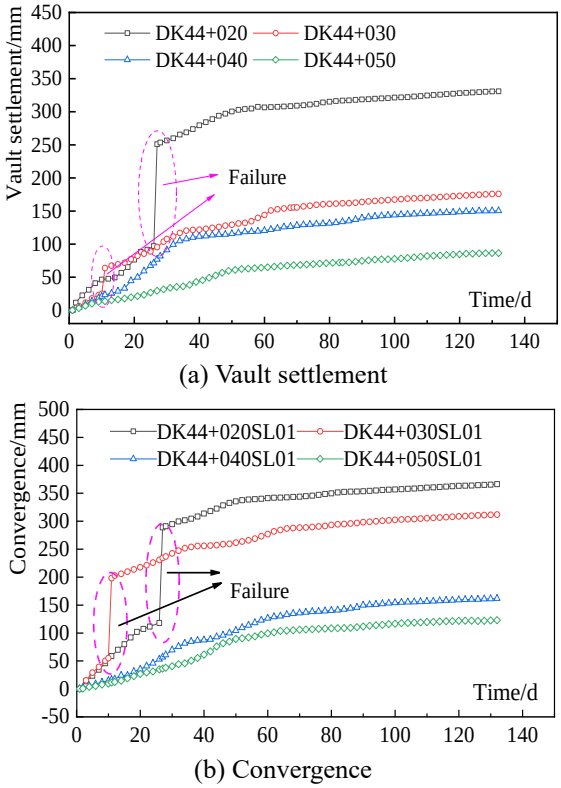

Fig. 3 Deformation of surrounding rock

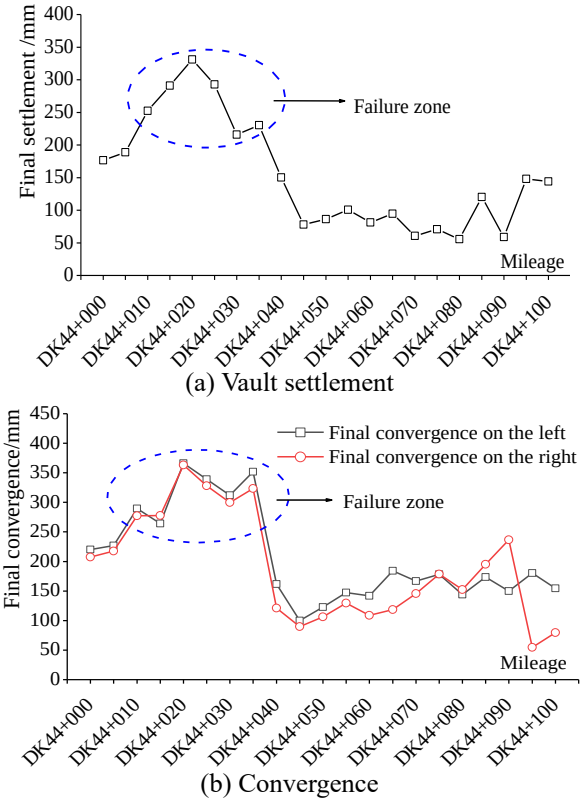

Fig. 4 Tunnel surrounding rock deformation at different length sections

The curves of tunnel vault settlement and convergence with time are shown in Fig. 3. The vault settlement and convergence of the four sections increase with time and finally reach stability. The final vault settlement values of DK44+040 section and DK44+050 section are 150.2 mm and 86.4 mm respectively. However, at the 27th day and the 11th day, the vault settlement values of DK44+020 section and DK44+030 section increase sharply and finally stabilize at 330.9 mm and 175.8 mm respectively.

3.2.2 Tunnel surrounding rock deformation at different mileage sections

The final vault settlement and horizontal convergence curves of the tunnel vault in the DK44+000~100 area are shown in Fig. 4. The final vault settlement value at DK44+010~035 is 55.7 mm-330.9 mm, and the final horizontal convergence value is 99.8 mm-366.2 mm. The vault settlement and horizontal convergence are the largest in the DK44+010~035 area. Combined with on-site investigation, it was found that a circumferential cracks were discovered at the DK44+028~032 section, and cracks were found at the left vault foot of the DK44+017~026 section, indicating that the first lining has already cracked and failed at the DK44+020 section and DK44+030 section.

Although there is no cracking phenomenon in the first lining at other sections, the average vault and horizontal convergence are 100 mm and 150 mm respectively, far greater than those of other ordinary tunnels. It shows that the vault settlement and horizontal convergence of tunnel excavation in water-rich fine sand strata are large, and appropriate deformation allowance in the construction should be set.

3.3 Liner pressure and stress

3.3.1 Liner pressure

The time-history curve of contact pressure between the first lining and the liner at DK43+981.3 section is shown in Fig. 5(a). The liner pressure increases with time, slowly increasing from 0-37d, rapidly increasing from 37-65d, and basically stabilizing after 65d. When the liner pressure stabilizes, the maximum pressure value is 99.7 kPa, located at the left wall of the tunnel, and the minimum pressure value is 27.7 kPa, located at the left arch foot. Overall, the liner pressure values are relatively small, and the liner is in a safe state. The maximum liner pressure value is 72.06 kPa higher than the minimum liner pressure value, with a large gap between the two. However, for the overall monitoring section, the liner pressure values at each monitoring point are relatively small, and none of them have reached the liner failure load, so the liner is in a safe state.

The time-history curve of liner pressure at DK44+009.3 monitoring section is shown in Fig. 5(b). The liner pressure is relatively small, which increases uniformly with time in the first 20 days, and then changes slowly and gradually stabilizes. The maximum liner pressure value at DK44+009.3 monitoring section is 148.76 kPa, which is located at the right wall, and the minimum value is 67.73 kPa, which is located at the right arch shoulder. The difference between the maximum and minimum lining pressure is 81.03 kPa, which is relatively large. However, compared with the whole monitoring section, the pressure values of each monitoring point are relatively small, and the liner is in a safe state.

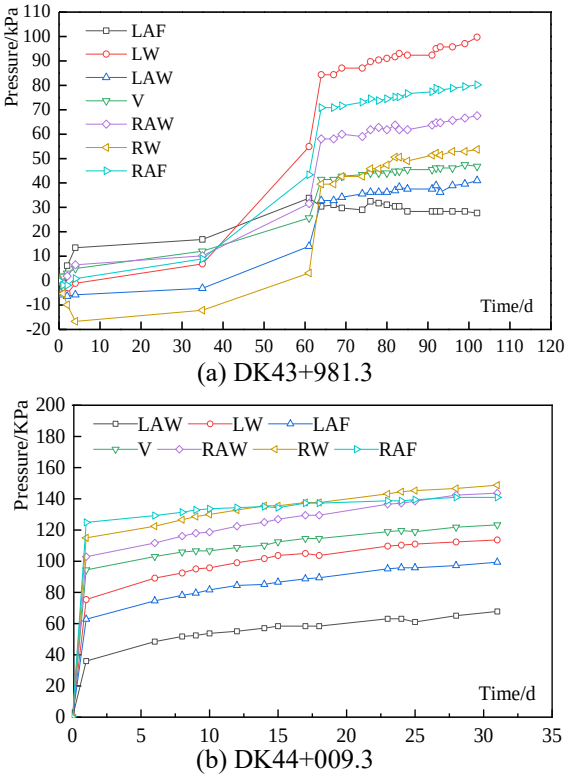

Fig. 5 Liner pressure

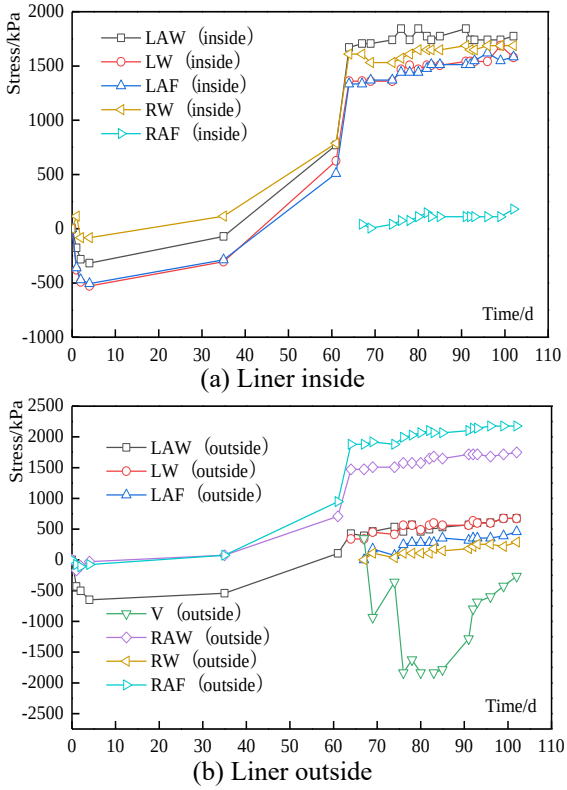

Fig. 6 liner stress of DK43+981.3

3.3.2 Liner stress

The stress time-history curves of the inner and outer sides of the DK43+981.3 monitoring section are shown in Fig. 6. The liner concrete mainly bears compressive stress. The stress gradually increases with time from 0-65d, and gradually stabilizes after 65d. When the stress of the liner concrete reaches a stable state, the maximum compressive stress on the outer side of the liner is 2.18 MPa, located at the right arch foot, and the maximum tensile stress is 0.29 MPa, located at the arch crown; the maximum compressive stress on the inner side of the liner concrete is 1.77 MPa, located at the left arch foot. The stress values do not exceed the compressive (tensile) limit of reinforced concrete, and the liner concrete is in a safe state.

The time-history curves of stress on the inner and outer sides of DK44+009.3 monitoring section are shown in Fig. 7. The stress on the outer side of liner concrete and the stress on the inner side uniformly increased rapidly in the first 25 days, and then increased slowly and gradually became stable.

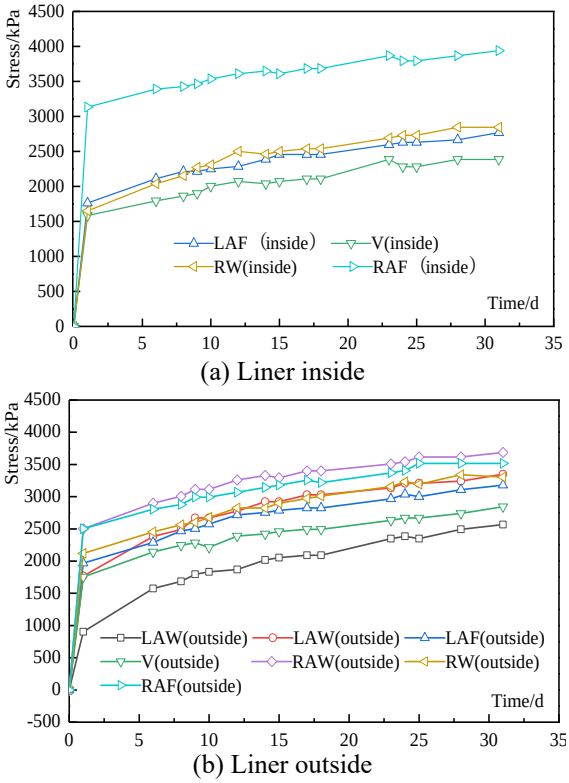

.Fig. 7 liner stress of DK44+009.3

3.3 Cause of destruction of first lining

On-site management staff found a circular crack at DK44+015 and a longitudinal crack at the left arch foot of DK44+017~026 section, as shown in Fig. 8. The first lining deformation section DK44+015~020 is located at the curtain grouting junction. During the excavation of DK44+018, the left arch waist and arch crown collapsed, forming a collapse cavity with dimensions of approximately 7 m×6 m×3 m in height, width, and depth. The collapse cavity was backfilled with radial grouting reinforcement treatment on site, with a grouting volume of approximately 29 m3. No further treatment was performed on the collapse cavity in the later stage.

Borehole sampling was conducted on the left side of the

(a) Circumferential crack

(b) Longitudinal crack

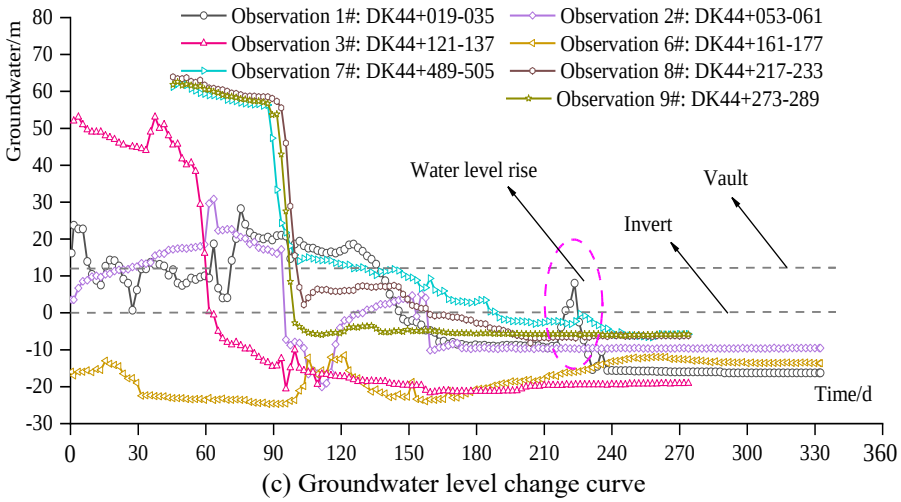

(c) Groundwater level change curve

Fig. 8 First lining cracking and grooundwater table change curve

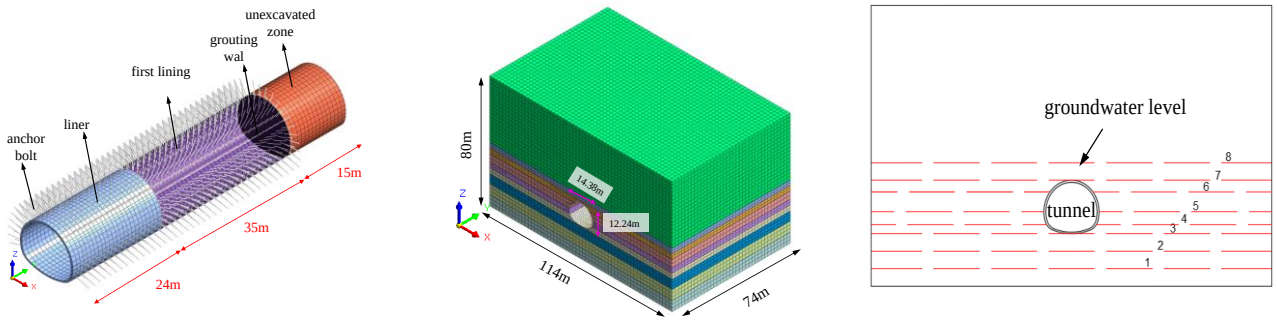

(a) Numerical model (b) Groundater table path

Fig. 9 Numerical mode and groundater table path

arch crown at the DK44+017 cross-section, and the water content of the surrounding rock in this range was detected to be 19.3%, far exceeding the normal construction allowable range. Further analysis shows that 3 m radial grouting reinforcement behind the planned initial support has not completely filled the caving cavity. the excessive water content of the surrounding rock led to instability of the surrounding rock, which leads to spalling of surrounding rock at the top of caving cavity and damages the first lining.

Observation wells were set up near multiple dewatering wells at the construction site, with each observation well able to observe water level changes within the working range of several different pumping wells. The specific water level changes of each observation well are shown in Fig. 8(c). Positive values represent water levels above the bottom of the tunnel invert, while negative values represent water levels below the bottom of the tunnel invert a. The tunnel height is 12.32 m. Observation well #1 can observe water level changes within the DK44+019~035 range, which is relatively close to the previously mentioned crack damage section and can be used as a reference. Combined with the water level changes of other observation wells, it can be seen that observation well #1 experienced a rebound in water level on the 216th day of operation. According to field observations, some of the dewatering wells in this area stopped working after the first lining construction being completed and did not continue to reduce water levels. Additionally, some dewatering wells were damaged and stopped operating, leading to a rebound in groundwater tables. The rebound in water levels caused the water content of the surrounding rock in this area to gradually increase, reducing the cohesive strength of the soil and increasing soil pressure. This ultimately led to compressive deformation of the first lining, resulting in longitudinal cracks and damage to the arch foot.

4. Analysis and discussion

Based on the on-site monitoring data and investigation, the groundwater table rise is the main reason for the cracking of the first lining. In this section, the finite element software Midas gts NX is used to establish a numerical model to further explore the failure mechanism of the first lining due to groundwater table rise. Before establishing the numerical model, the characteristics of the fine sand stratum of the Xiangshan Tunnel are determined through sieving

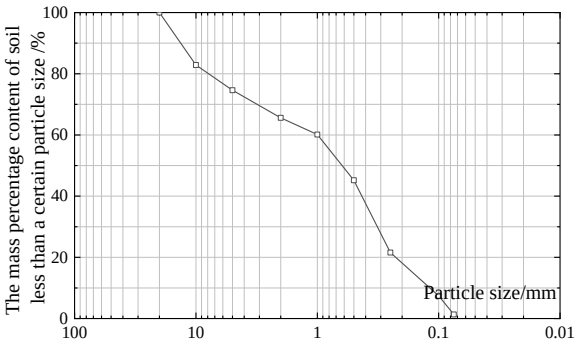

Fig. 10 Particle size distribution

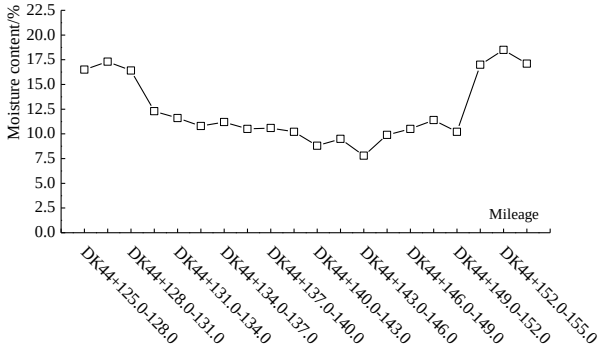

Fig. 11 Moisture content of sand samples

test, density test, moisture content test, compression test and direct shear test, providing data support for numerical simulation.

4.1 Numerical model and mechanical parameters of materials

4.1.1 Numerical model

The Xiangshan Tunnel DK43+958~DK44+515 section, the shallowest buried depth of this section of the tunnel is 120 meters, and the deepest buried depth is 150 meters. The DK44+134~208 section is selected as the research object. The width of the tunnel section is 14.38 m and the height is 12.24 m. The disturbance range of tunnel excavation is 3~5 times the tunnel diameter, and the groundwater table is 18 m below the invert bottom. The numerical model, the size in the X direction is 114 m, the size in the Y direction is 74 m, and the size in the Z direction is 70 m. There is 15 m of unexcavated core soil in front of the tunnel face. The tunnel face is supported by a grouting wall, the first lining section is 24 m long, and the liner section is 35 m long. The surrounding rock adopts the Mohr-Coulomb model, and the shotcrete, first lining, grouting wall and anchor bolt adopt the elastic model. The surrounding rock and liner are simulated by three-dimensional solid elements; the shotcrete structure and grouting wall are simulated by plate elements, the thickness of the shotcrete surface layer is 28 cm, and the thickness of the grouting wall is 1.5 m; the anchor bolt structure is simulated by a one-dimensional linear element, and the diameter of the anchor bolt is 22 mm and the length is 4 m. The boundary conditions are displacement constraints, that is, horizontal constraints are applied to the surroundings, and fixed constraints are applied to the bottom, the top surface of the model is a free surface, and the numerical model is shown in Fig. 8. To compare the effects of different groundwater tables on the tunnel structure, a total of 8 groundwater tables were set, including -12 m below the invert bottom, -6 m below the invert bottom, invert bottom water level, arch foot water level, arch waist water level, arch shoulder water level, vault water level, and 4 meters above the vault water level, as shown in Fig. 9.

4.1.2 Material parameters

The natural density test of undisturbed soil was carried out by using the ring knife method, and the average natural density of the fine sand sample was 1.86 g/cm3. The grain gradation of fine sand in front of the tunnel face is shown in Fig. 10. The particle size of the sand sample is greater than 0.075 mm, and the particle mass exceeds 85% of the total mass. The sand sample could be regarded as fine sand. The sand sample has a coefficient of uniformity Cu>5, which is non-uniform soil according to relevant specifications, and its curvature coefficient 1<Cc<3. The sand sample has good continuity of soil particle size gradation and good particle gradation.

The water content of fine sand in DK44+125.0~155.0 section is shown in Fig. 11. The water content of sand samples ranges from 7.8% to 18.5%, and gradually decreases in DK44+125.0~156.0 section. The water content in DK44+143.0~146.0 section is the lowest, only 7.8%, so this section is a water-rich area. Then the water content of sand samples gradually increases, reaching the maximum value of 18.5% in DK44+152.0~155.0 section.

Six groups of powder fine sand samples with water content of 8%, 10%, 12%, 14%, 16% and 18% were prepared respectively. The compression modulus of sand samples with different water content was measured by 1 h rapid consolidation test, and the results are shown in Fig. 12. The compression modulus of sand samples varies with different water content. Under the same vertical pressure condition, the compression modulus increases first and then decreases with the increase of water content of sand samples. When the water content of sand samples is 12%, the compression modulus reaches the maximum, which is 45.53 MPa. When the water content of sand samples is 8%, the compression modulus is the smallest, which is 23.32 MPa.

Prepared 6 groups of powder fine sand samples with water content of 8%, 10%, 12%, 14%, 16% and 18% respectively. The cohesion c and internal friction angle φ of sand samples were obtained by quadruple quick shear test, and the results are shown in Fig. 13. The cohesion and internal friction angle of sand samples increase first and then decrease with the increase of water content. When the water content is 12%, the shear strength is the largest. At this time, the cohesion of sand samples is 15.27 kPa, and the internal friction angle is 33.07°. When the water content of sand samples is 18%, the cohesion and internal friction angle are the smallest, which are 10 kPa and 28.07° respectively. Therefore, comparing the mechanical properties of sand samples under different water contents, the engineering mechanical properties of sand samples with water content of 12% are the best.

Table 1 Physical and mechanical parameters

Name	Unit weight γ/(kN·m^{-3})	Cohesion c/kPa	Internal friction angle φ/°	Poisson's ratio/ν	Elasticity modulus E/MPa
Fine sand	18.6	15.27	33.07	0.35	7×10^{1}
Fine sand (12%)	20.64	15.27	33.07	0.35	2.52×10^{1}
First lining	24	-	-	0.2	3.285×10^{4}
Grouting wall	24	-	-	0.2	2.8×10^{4}
Liner	24	-	-	0.2	3.15×10^{4}
Anchor bolt	77	-	-	0.3	2.1×10^{5}

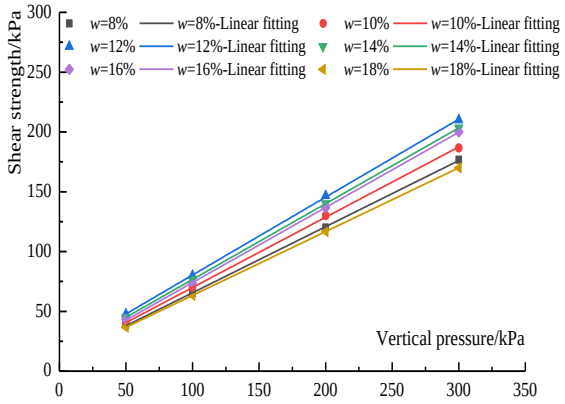

Fig. 12 Sand sample direct shear test

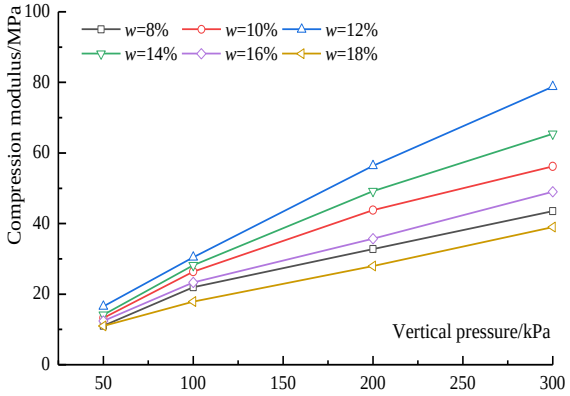

Fig. 13 Change curve of compression modulus

Based on the above test , the fine sand with a moisture content of 12% was selected to simulate the surrounding rock. The physical and mechanical parameters of the surrounding rock are shown in Table 1.

4.2 Deformation of surrounding rock

The displacement contour of the tunnel in the x direction is shown in Fig. 14. With the rise of groundwater table, the stratum around the tunnel will produce horizontal displacement in the x direction. When the groundwater table is below the invert bottom, the horizontal displacement changes little. When the water level exceeds the invert bottom, the change becomes obvious, and the higher the water level, the more obvious the change. The horizontal displacement in the x direction is mainly concentrated at the arch waist and arch foot, and the horizontal displacement of the liner section changes little, while the horizontal displacement of the first lining section changes greatly. It can be seen that the liner can effectively control the deformation of the surrounding rock after being applied.

The displacement contour of tunnel in y direction is shown in Fig. 15. Horizontal displacement in y direction occurs at the position of tunnel face, and the surrounding rock at the tunnel face bulges towards the inside of the tunnel. It also changes significantly when the groundwater table reaches the invert bottom, but the overall deformation is small. It shows that the application of grouting wall can effectively control the stability of the surrounding rock of the tunnel face. The horizontal displacement in y direction at the junction of first lining and liner is relatively large, so it is necessary to strengthen the monitoring and measurement at the junction of first lining and liner during the construction process.

The displacement contour of the tunnel in z direction is shown in Fig. 16. With the recovery of groundwater table, the vertical displacement generated by the surrounding strata of the tunnel is manifested at the invert bottom and the vault crown, with the maximum located at the middle of the first lining section of the vault crown. The vertical displacement of the first lining section is significantly larger than that of the liner section. Therefore, the application of liner can effectively improve the stability of the surrounding rock. Compared with the horizontal displacement, the vertical displacement of the whole tunnel is much larger. Unlike the horizontal displacement, the vertical displacement also has significant changes when the water level is at the invert bottom, and the higher the water level, the greater the change.

4.3 Deformation and force of the first lining

4.3.1 Deformation of the first lining

The evolution law of vertical deformation and horizontal deformation of the first lining is shown in Fig. 17. During the whole process of groundwater table rise, the deformation of the soil around the first lining is mainly dominated by vertical displacement, and the horizontal displacement changes little. The vertical deformation of the soil around the first lining is mainly settlement, with the largest settlement at the vault and the smallest settlement at the invert bottom. The deformation laws of the vault and the two sides of the arch waist are similar. As the groundwater

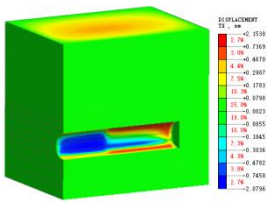
(a) -12 m below the invert

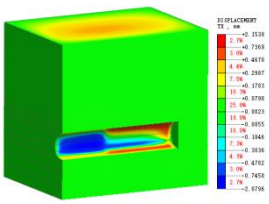
(b) -6 m below the invert

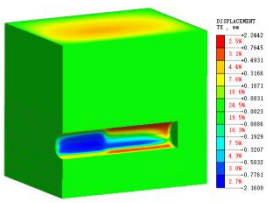
(c) Invert

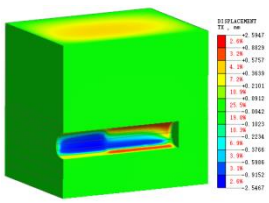
(d) Arch foot

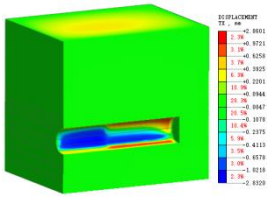
(e) Arch waist

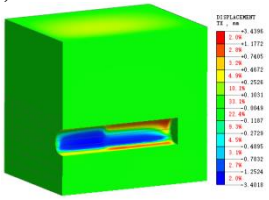
(f) Arch shoulder

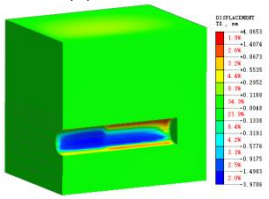
(g) Vault

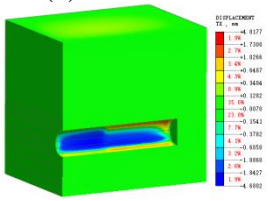
(h) 4 m above the vault

Fig. 14 Horizontal displacement contour in *x* direction

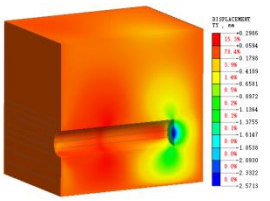
(a) -12 m below the invert

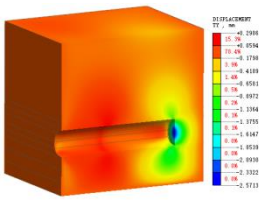
(b) -6 m below the invert

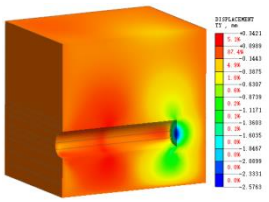
(c) Invert

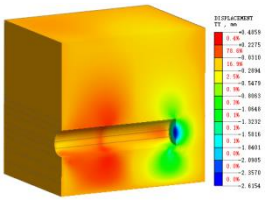
(d) Arch foot

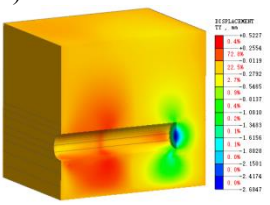
(e) Arch waist

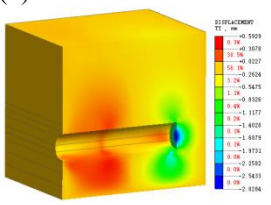
(f) Arch shoulder

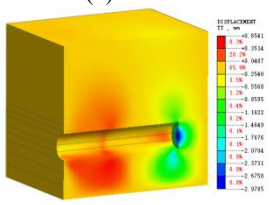
(g) Vault

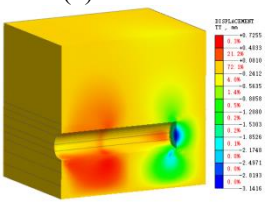
(h) 4 m above the vault

Fig. 15 Horizontal displacement contour in y direction

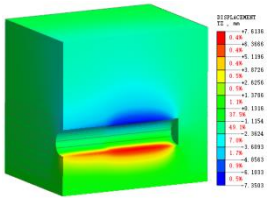
(a) -12 m below the invert

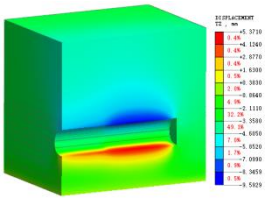
(b) -6 m below the invert

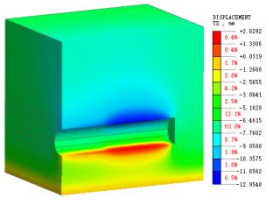
(c) Invert

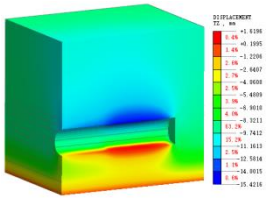
(d) Arch foot

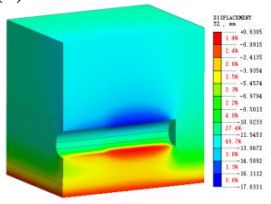
(e) Arch waist

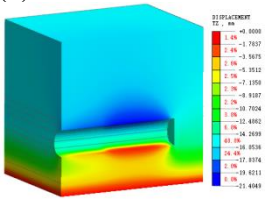
(f) Arch shoulder

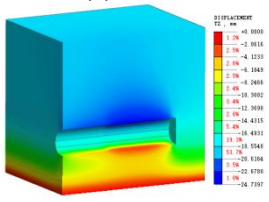
(g) Vault

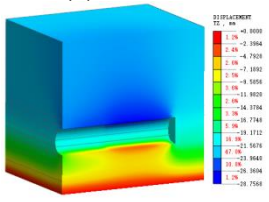
(h) 4 m above the vault

Fig. 16 Horizontal displacement contour in *z* direction

table gradually rises, the settlement rate gradually increases. When the groundwater table reaches the invert bottom, under the influence of buoyancy, the settlement rate decreases, and the invert bottom is the most obvious. The overall horizontal displacement of the invert bottom and the vault is very small, and the horizontal displacement trends of the two sides of the arch waist are the same. When the groundwater table reaches the arch bottom, there is a significant horizontal displacement on both sides of the arch waist, and the rate of increase in horizontal displacement

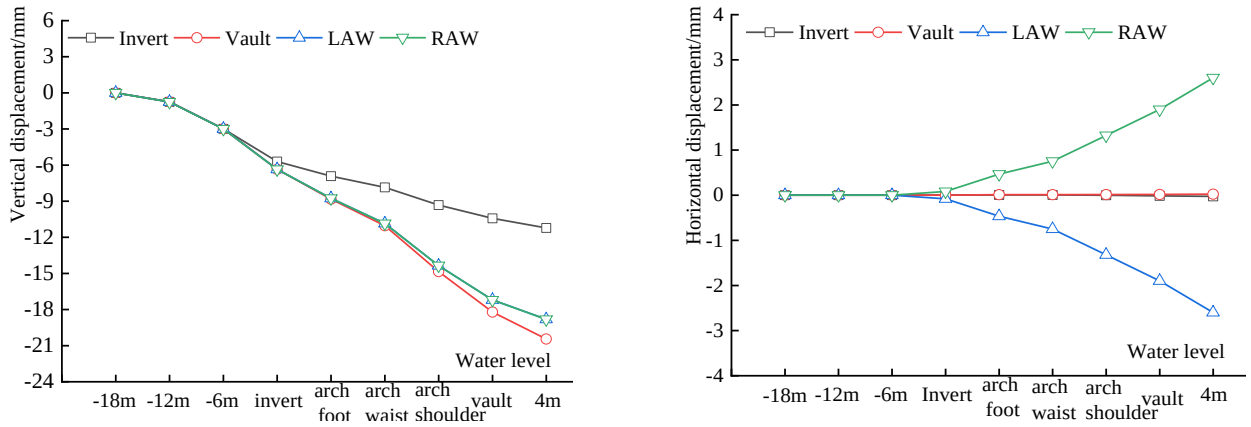

(a) Vertical displacement (b) Horizontal displacement

Fig. 17 First lining displacement

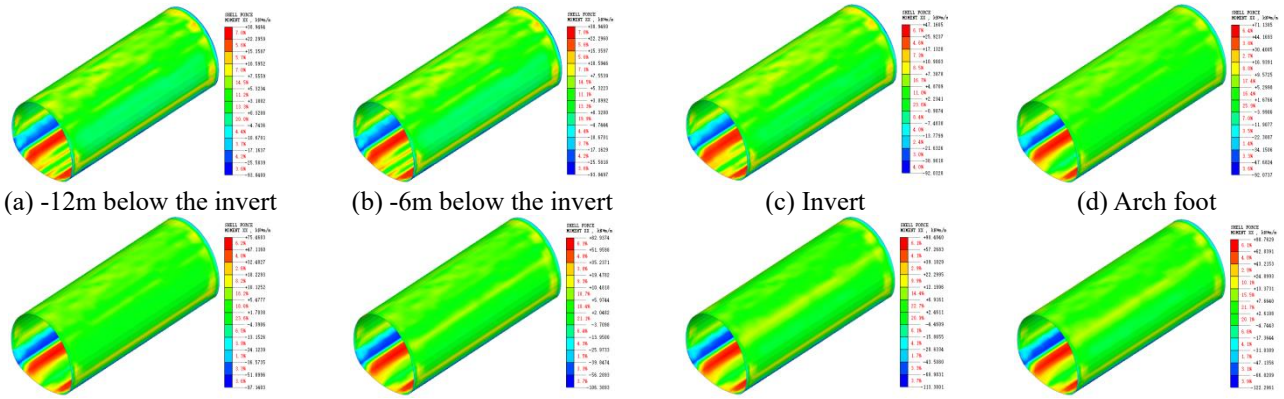

(a) -12m below the invert (b) -6m below the invert (c) Invert (d) Arch foot

(e) Arch waist (f) Arch shoulder (g) Vault (h) 4m above the vault

Fig. 18 Bending moment contour

gradually rises, indicating that when the groundwater table exceeds the invert bottom. It will have a greater impact on the horizontal deformation of the surrounding rock, and the higher the groundwater table, the greater the impact.

4.3.2 First lining moment and axial force

The contour of the first lining bending moment is shown in Fig. 18. The bending moment of the vault and invert bottom is positive. The bending moment of both sides of the arch is negative. The first lining shows an overall flattened state. The maximum positive bending moment is on both sides of the invert, and the maximum negative bending moment is at the arch foot. There is a large positive bending moment on both sides of the invert, and there is a large negative bending moment in the arch foot range. Therefore, there is a significant positive and negative bending transition between the two, which will bear a large shear stress. Excessive stress will cause damage to the first lining, resulting in cracks. When the groundwater table is below the invert bottom, the first lining bending moment value changes relatively little, with a maximum absolute value increase of 21.3% and a minimum absolute value increase of 1.1%. When the groundwater table rises from the invert bottom to the vault, the bending moment value changes significantly, with a maximum absolute value increase of 91.7% and a minimum absolute value increase of 23.3%. The groundwater table in this range has a greater impact on the first lining, especially after the groundwater table reaches the arch waist, the bending moment changes most obviously. When the groundwater table continues to rise by 4 m, the change in bending moment value is still large. The bending moment of the first lining will be greatly affected by the water level beyond the vault.

The axial force contour of the first lining is shown in Fig. 19. The axial force near the tunnel face is positive, and there is a stress concentration phenomenon. The axial force at other positions is negative, and the tunnel is in a compressed state overall. The axial force distribution in the range of the invert bottom and the vault is relatively uniform. The distribution of the axial force values in the range from the arch foot to the arch shoulder is extremely uneven, and the axial force values vary greatly. In the early stage of immersion, the change of the axial force of the first lining is very small, and the maximum increase is only 0.2%. The change of groundwater table in this range has little effect on the first lining. When the groundwater table rises from the vault bottom to the vault, the axial force changes significantly, with an increase of 19.1%. The change of groundwater table in this range has a greater impact on the first lining. Especially when the groundwater

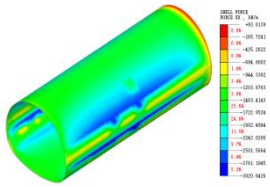

(a) -12 m below the invert

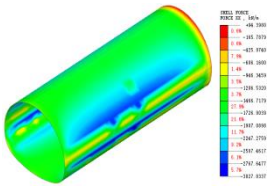

(b) -6 m below the invert

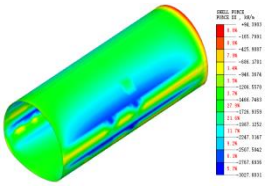

(c) Invert

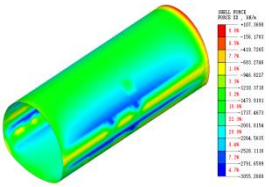

(d) Arch foot

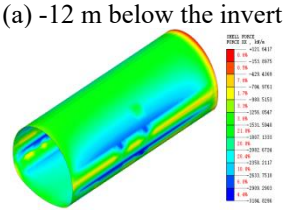

(e) Arch waist

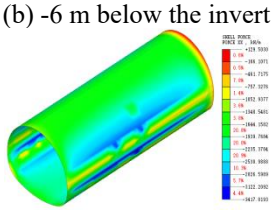

(f) Arch shoulder

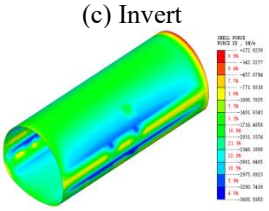

(g) Vault

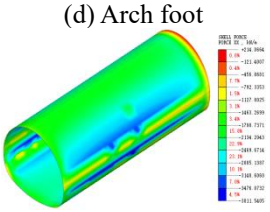

(h) 4 m above the vault

Fig. 19 Axial force contour

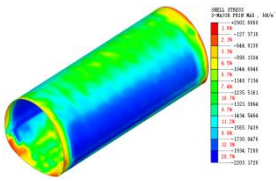

(a) -12 m below the invert

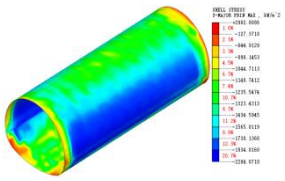

(b) -6 m below the invert

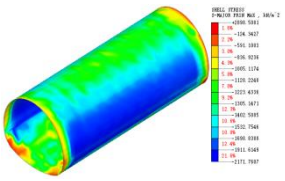

(c) Invert

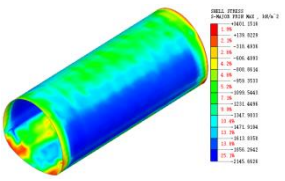

(d) Arch foot

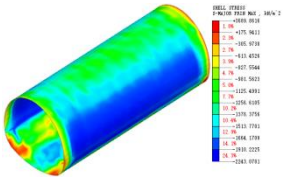

(e) Arch waist

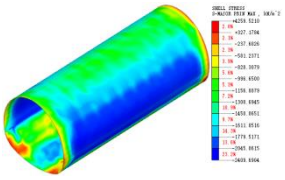

(f) Arch shoulder

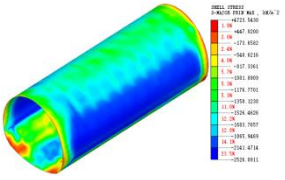

(g) Vault

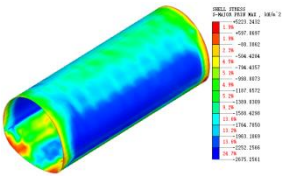

(h) 4 m above the vault

Fig. 20 Maximum principal stress contour

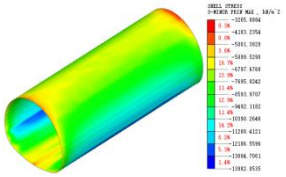

(a) -12m below the invert

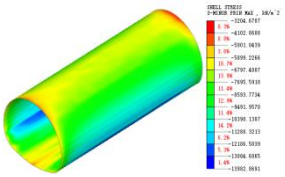

(b) -6 m below the invert

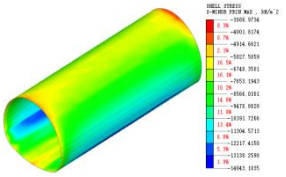

(c) Invert

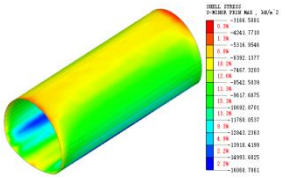

(d) Arch foot

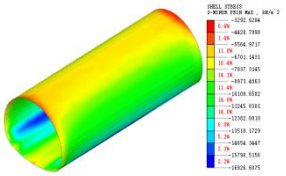

(e) Arch waist

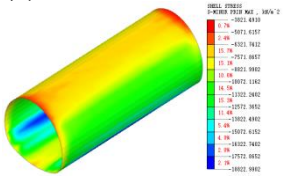

(f) Arch shoulder

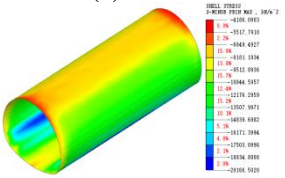

(g) Vault

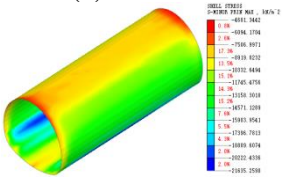

(h) 4 m above the vault

Fig. 21 Minimum principal stress contour

table reaches the arch waist, the axial force increases significantly. When the groundwater table continues to rise by 4m after exceeding the vault, the maximum axial force value increases by 5.7%, and the change range is still large, indicating that the groundwater table still has a great impact on the axial force of the first lining after exceeding the vault.

4.3.3 The stress of first lining

The maximum principal stress contour and the minimum principal stress contour of the first lining are shown in Figs. 20 and 21. The maximum principal stress and the minimum principal stress of the first lining are symmetrically distributed along the tunnel midline. The tunnel is mainly compressed. As can be seen from Fig. 20, the minimum value of the maximum principal stress is at the arch waist, and stress concentration occurs at the arch foot position near the tunnel face, with very high stress up to 2.3 MPa. This phenomenon also exists at the interface between the first lining and the liner. As can be seen from

Fig. 21, the maximum value of the minimum principal stress is at the arch foot, and the maximum value is at the vault near the tunnel face. Except for the uneven stress distribution at the front and rear ends, the stress of the first lining is relatively uniform.

During the process of water level rising to the invert bottom in the early stage of immersion, both the maximum and minimum principal stresses changed very little, and the maximum compressive stress of the first lining only increased by 0.06 MPa. This shows that when the groundwater table is below the vault bottom, it will not have a significant impact on the stability of the first lining.The first lining is in a safe state. When the groundwater table rises from the invert bottom to the vault, the maximum compressive stress increment of the first lining is as high as 6.13 MPa, increasing by 43.66%. The higher the groundwater table, the greater the increment and the greater the impact on the stability of the first lining. It should be noted that when the groundwater table reaches the arch waist, the maximum compressive stress at the arch foot reaches 16.93 MPa, exceeding the first lining ultimate strength, and damage will occur, forming longitudinal cracks. When the groundwater table continues to rise 4 m from the vault, the maximum compressive stress increases by 7.3%, which will accelerate the damage speed of the first lining and increase the damage scope of the first lining.

4.4 Construction proposal

In summary, the groundwater table rebound will increase the deformation and stress of the first lining, but it will not have a great impact on the liner. Therefore, in the actual construction process, continuous dewatering should be required to ensure that the groundwater table is below the first lining. Secondly, in the construction process, the junction of the first lining and the liner is easy to deformation and uncoordinated. The first lining may deformation and crack. Therefore, the monitoring and investigation of this area should be strengthened during the construction process. Finally, the length of the first lining section should be shortened as much as possible during the construction process to prevent the first lining from cracking.

5. Conclusions

Taking the DK43+958~DK44+515 section of the Xiangshan Tunnel of Zhonglan Railway as a case study, the effect of groundwater table rebound on the stability of tunnel structure was investigated.The suggestions and main conclusions obtained during the construction are as follows:

- The groundwater table rebound will cause a large vertical settlement of the support structure. When the groundwater table reaches the invert bottom, the tunnel has a tendency to move to the right, but the horizontal displacement is very small. The groundwater table rebound will cause greater extrusion deformation of the tunnel face, and the application of grouting wall can effectively improve the stability of the tunnel face.
- During the whole process of groundwater table rebound, the first lining is in a flattened state. When the groundwater table exceeds the invert bottom, the bending moment and axial force of the first lining change significantly. Especially when the groundwater table reaches the arch waist, there is a transition of positive and negative bending moment near the arch foot of the first lining, which will bear a large shear stress. Excessive stress will cause damage to the arch foot. Stress concentration will occur near the tunnel face.
- After the groundwater table is higher than the invert bottom, the maximum principal stress and the minimum principal stress of the first lining will increase significantly, and the higher the water level, the greater the principal stress. When the groundwater table reaches the arch waist, the minimum principal stress at the arch foot of the first lining exceeds its ultimate strength and fails. If the groundwater table continues to rise, it will accelerate the failure rate of the first lining and increase the scope of damage.
- The increase of surrounding rock moisture content caused by rising groundwater table is the main reason leading to the failure of the first lining. By reducing the groundwater table, adding steel arch to the damaged section of the first lining, and carrying out radial grouting, the cracking problem of the first lining can be effectively solved and the security of tunnel construction can be provided.

Acknowledgements

The present work is subsidised and supported by the National Natural Science Foundation of China (Nos. 52308375, 52178393), the China Postdoctoral Science Foundation(2024MD753967), the Shaanxi Province Postdoctoral Science Foundation (2023BSHEDZZ273), the Science and Technology Innovation Team of Shaanxi Innovation Capability Support Plan (No. 2020TD005). The authors gratefully acknowledge the financial supports.

References

Chen, R., Yin, X., Tang, L. and Chen, Y. (2018), "Centrifugal model tests on face failure of earth pressure balance shield induced by steady state seepage in saturated sandy silt ground", *Tunn. Undergr. Sp. Tech.*, **81**, 315-325. https://doi.org/10.1016/j.tust.2018.06.031.

Cheng, C., Jia, P.J., Ni, P.P., Wang, Y., Zhao, W. and Guan, Y. (2023), "Upper bound analysis of longitudinally inclined EPB shield tunnel face stability in dense sand strata", *Transp. Geotech.*, **41**, 1-15. https://doi.org/10.1016/j.trgeo.2023.101031.

Ding, L.Y., Yu, H.L., Li, H., Zhou, C., Wu, X.G. and Yu, M.H. (2012), "Safety risk identification system for metro construction on the basis of construction drawings", *Automat. Constr.*, **27**, 120-137. https://doi.org/10.1016/j.autcon.2012.05.010.

Eskandari, F., Goharrizi, K.G. and Hooti, A. (2018), "The impact of epb pressure on surface settlement and face displacement in intersection of triple tunnels at mashhad metro", *Geomech. Eng.*, **15**(2), 769-774. https://doi.org/10.12989/gae.2018.15.2.769.

Fan, H.B., Xu, Q., Lai, J.X., Liu, T., Zhu, Z., Zhu, Y. and Gao, X.

(2023), "Stability of the loess tunnel foundation reinforced by jet grouting piles and the influence of reinforcement parameters", *Transp. Geotech*., **40**, 1-16. https://doi.org/10.1016/j.trgeo.2023.100965.

Kang, Y., Liu, Q., Cheng, Y. and Liu, X. (2016), "Combined freeze-sealing and new tubular roof construction methods for seaside urban tunnel in soft ground", *Tunn. Undergr. Sp. Tech*., **58**(9), 1-10. http://dx.doi.org/10.1016/j.tust.2016.04.001.

Khezri, N., Mohamad, H. and Fatahi, B. (2016), "Stability assessment of tunnel face in a layered soil using upper bound theorem of limit analysis", *Geomech. Eng*., **4**(11), 471-492. https://doi.org/10.12989/gae.2016.11.4.471.

Kirsch, A. (2010), "Experimental investigation of face stability of shallow tunnels in sand", *Acta Geotech*., **5**(1), 43-62. https://doi.org/10.1007/s11440-010-0110-7.

Lei, M., Lin, D., Huang, Q., Shi, C. and Huang, L. (2020), "Research on the construction risk control technology of shield tunnel underneath an operational railway in sand pebble formation: A case study", *Eur. J Environ, Civ, Eng*., **24**(10), 1558-1572. https://doi.org/10.1080/19648189.2018.1475305,

Li, Y.H., Tang, X.J. and Yang, Y.F. (2023), "Characterization of face stability of shield tunnel excavated in sand-clay mixed ground through transparent soil models", *Geomech. Eng*., **33**(5), 439-451. https://doi.org/10.12989/gae.2023.33.5.439.

Liang, Y., Chen, X., Yang, J., Zhang, J. and Huang, L. (2020), "Analysis of ground collapse caused by shield tunnelling and the evaluation of the reinforcement effect on a sand stratum", *Eng. Fail. Anal*., **115**, 1-13. https://doi.org/10.1016/j.engfailanal.2020.104616.

Liu, N., Li, N., Li, G., Zhang, Z. and Mu, Y. (2018), "Deformation and collapse mechanisms of water-rich soil tunnels", *Soil Mech, Found, Eng*., **54**(6), 384-394. https://doi.org/10.1007/s11204-018-9485-5.

Liu, X., Wang, F., Huang, J., Wang, S., Zhang, Z. and Nawnit, K. (2019), "Grout diffusion in silty fine sand stratum with high groundwater level for tunnel construction", *Tunn. Undergr. Sp. Tech*., **93**, 1-11. https://doi.org/10.1016/j.tust.2019.103051.

Long, Y. and Tan, Y. (2020), "Soil arching due to leaking of tunnel buried in water-rich sand", *Tunn. Undergr. Sp. Tech*., **95**, 1-18. https://doi.org/10.1016/j.tust.2019.103158.

Qiu, J.L., Liu, D.D., Zhao K., Lai, J., Wang, X., Wang, Z. and Liu, T. (2024), "Influence spatial behavior of surface cracks and prospects for prevention methods in shallow loess tunnels in China", *Tunn. Undergr. Sp. Tech*., **143**, 105453. https://doi.org/10.1016/j.tust.2023.105453.

Oreste, P.P. and Dias, D. (2012), "Stabilisation of the excavation face in shallow tunnels using fibreglass dowels", *Rock Mech. Rock Eng*., **45**(4), 499-517. https://doi.org/10.1007/s00603-012-0234-1.

Park, J.K. (2022), "Reliability analysis of tunnel face stability considering seepage effects and strength conditions", *Geomech. Eng*., **3**(2), 9331-338. https://doi.org/10.12989/gae.2022.29.3.331.

Song, Z., Shi, G., Zhao, B., Zhao, K. and Wang, J. (2020), "Study of the stability of tunnel construction based on double-heading advance construction method", *Adv. Mech. Eng*., **12**(1), 1-17. https://doi.org/10.1177/1687814019896964.

Tan, Z., Zhou, Z., Kong, H., Zhao, B. and Zhao, J. (2021), "Single excavation face method for super large span bifurcated tunnels", *P I Civil Eng. Geotec*., 1, 1-46. https://doi.org/10.1680/jgeen.20.00222.

Tian, X., Song, Z., Wang, H., Zhang , Y. and Wang, J. (2022), "Evolution characteristics of the surrounding rock pressure and construction techniques: A case study from taoshuping tunnel", *Tunn. Undergr. Sp. Tech*., **125**, 1-17. https://doi.org/10.1016/j.tust.2022.104522.

Wang, H.Z., Song, Z.P., Tian, X.X., Wen, B. and Zhang, Y.W. (2024), "Investigation of the stress and strain distribution in the surrounding soil of a tunnel induced by the double-heading at bottom method", *Int. J. Civ. Eng*., 1-19. https://doi.org/10.1007/s40999-024-00958-1.

Wang, L., Han, K., Xie, T. and Luo, J. (2019), "Calculation of limit support pressure for epb shield tunnel face in water-rich sand", *Symmetry*, **11**(9), 1-16. https://doi.org/10.3390/sym11091102.

Yang, W., Li, L., Shang, Y., Yan, Q., Fang, Y., He, C. and Xu, Z. (2018), "An experimental study of the dynamic response of shield tunnels under long-term train loads", *Tunn. Undergr. Sp. Tech*., **79**(9), 67-75. https://doi.org/10.1016/j.tust.2018.04.031.

Yang, Y.S., Zhang, S.H., Zhang, J.H., Yuan, Y., Li, C. and Yu, H. (2022), "Effect of excitation frequency on segmental tunnels in sand using 1g shaking table tests", *Transp. Geotech*., **34**, 1-12. https://doi.org/10.1016/j.trgeo.2022.100750.

Ye, F., Qin, N., Gao, X., Quan, X., Qin, X. and Dai, B. (2019), "Shield equipment optimization and construction control technology in water-rich and sandy cobble stratum: a case study of the first yellow river metro tunnel undercrossing", *Adv. Civ. Eng*., **1**, 1-12. https://doi.org/10.1155/2019/8358013.

Yin, Z.Y., Wang, P. and Zhang, F.S. (2020), "Effect of particle shape on the progressive failure of shield tunnel face in granular soils by coupled FDM-DEM method", *Tunn. Undergr. Sp. Tech*., **100**, 1-16. https://doi.org/10.1016/j.tust.2020.103394.

Zan, W.B., Lai, J.X., Zhang, W.J., Yang, Q., Qin, Y. and Su, X. (2024), "Experimental and applied research on similar materials to granular mixtures for the solid-liquid coupling model test of an underwater tunnel", *Constr. Build. Mater*., **416**, 135170. https://doi.org/10.1016/j.conbuildmat.2024.135170.

Zhang, W., Zhang, Q. and Cao, W. (2021), "Study on stress and deformation of bolt joints of shield tunnel under static and seismic action", *KSCE J. Civ. Eng*., **25**, 3146-3159. https://doi.org/10.1007/s12205-021-1339-4.

JS